Potential of Magnetized Clay Particles on the Adsorption of Copper in Aqueous Solutions

Ntiyiso N Tshabalala and Elvis Fosso-Kankeu

***Abstract*— This study investigated the efficacy of magnetized bentonite clay particles (MBCP) in adsorbing copper ions from aqueous solutions, addressing the pressing environmental challenge posed by industrial copper discharge. Heavy metals like copper are prevalent pollutants originating from various industries, posing significant risks to human health and ecosystems. The research focused on optimizing the adsorption process by examining the influence of factors such as pH levels, contact time, and initial copper concentrations. Experimental results demonstrated that magnetized bentonite clay particles (MBCP) achieved a maximum adsorption capacity of 60% at an optimal contact time of 45 minutes and an initial concentration of 500 ppm. Utilizing a combination of experimental methods including kinetic modelling and adsorption isotherms, the study evaluated the performance of MBCP in terms of its adsorption capacity and separation efficiency. Kinetic modelling indicated that the adsorption process followed pseudo-second-order kinetics, suggesting a chemisorption mechanism. Results indicated that magnetization enhanced bentonite clay's properties, facilitating improved copper ion recovery while promoting environmental sustainability through cost-effective and efficient wastewater treatment solutions.**

***Keywords*— Magnetized clay particles, lithium, adsorption, wastewater.**

I. INTRODUCTION

Heavy metals such as copper(Cu) are often found in various industrial wastewater, categorizing them as prevalent pollutants. These metals can originate from sectors such as metal plating, electroplating, mining operations, acid mine drainage, fertilizer creation, battery production, dye manufacturing, the chemical and pharmaceutical industries, and electronic device construction. Many heavy metals are highly toxic and do not decompose naturally; thus, it is crucial to remove them from polluted water bodies to meet the growing demands for environmental quality regulations [1].

Copper is crucial in the production of solar panels, wind turbines, and other renewable energy technologies, it also is used in building materials, such as pipes, fittings, and roofing, due to its corrosion resistance and durability.

Adsorption technology has emerged as a promising alternative to traditional metal extraction methods [2-9]. Bentonite clay, a naturally abundant and environmentally friendly material, shows great potential for copper adsorption due to its high specific surface area, cation exchange capacity, and chemical stability. However, separating and recycling bentonite clay particles after adsorption remains a challenge.

Recent studies have explored the magnetization of bentonite clay particles to improve their separation and recycling efficiency. Magnetized bentonite clay particles can be easily separated from aqueous solutions using a magnetic field, reducing the need for energy-intensive centrifugation and filtration processes. In addition, the magnetization of bentonite clay particles can improve their copper adsorption capacity and selectivity.

Despite these advances, further research is still needed to optimize the synthesis and application of magnetized bentonite clay particles for copper adsorption. This project aims to study the influence of magnetization on the adsorption properties of bentonite clay particles and explore their potential for sustainable copper mining.

Although the demand for copper is increasing, the process of mining and recovering it remains inefficient and harmful to the environment. Bentonite clay, a natural and abundant material, shows promise for copper adsorption, but its low adsorption capacity and slow kinetics limit its applicability. Recent studies have demonstrated that magnetized bentonite clay particles can improve their copper adsorption properties. However, the optimal magnetization conditions, particle size, and surface chemistry to maximize copper adsorption remain unknown [10].

The aim of this research is to investigate the potential of magnetised clay particles on the adsorption of lithium in aqueous solutions.

II. METHODOLOGY

A. Synthesis & characterisation of MBCP

To prepare the magnetised bentonite clay particles, raw bentonite clay was collected from the analytical lab. 50g of the clay was weighed as well as 20g magnetite and were heterogeneously mixed with 80ml of deionized water. The mixture was then put on a magnetic stirrer for about 3 hours. The mixture was stirred at 300rpm, this helped mix the bentonite clay with the magnetite nanoparticles. The mixture was then washed using deionized water and this was done to lower the Ph to a neutral level. The bentonite was now magnetised and was left in the oven for 24 hours to dry. It was

Ntiyiso N Tshabalala, Department of Metallurgy at the University of Johannesburg in South Africa.

Elvis Fosso-Kankeu, Department of Metallurgy at the University of Johannesburg in South Africa

then stored in an air-tight

The clay particles were characterised using XRD, SEM-EDS as well as BET analysis. The crystalline structure of the adsorbent was studied or identified using this technique. SEM helped examine the morphology and surface features of the clay particles. It also identified surface modifications and copper deposition on the clay particles. On the other hand, BET analysis was used to measure the surface area of the clay particles as well as determined the pore size and volume distribution. By this analysis, the adsorption capacity and the potential of the clay particles for copper ions.

B. Chemicals and Adsorption Experiments

An accurate amount of powdered copper sulphate (CuSO4.5H2O) was dissolved to prepare a stock solution of 1000ppm concentration. The experiments were conducted at room temperature and were put on a shaker at 200rpm. The stock solution was brought to concentrations (100, 200, 300, 400 and 500ppm) by simply diluting the stock solution to the adequate concentrations. The adsorbent dosage used for each concentration was kept being 0.2g. The results of the effect of the experiment concerning the initial metal concentration were examined at contact time from 0 to 40 minutes. The mixture of 0.2g MBCP and copper sulphate at different concentrations and contact time were left on the shaker and after the contact time has been reached, the mixture was filtered using filter papers and funnels to remove the solid particles from the liquid. The liquid was taken for AAS to see how much of the adsorption took place. And the removal efficiency was calculated by :

%RE= (Ci-Co)/Ci × 100.

III. RESULTS AND DISCUSSION

A. Effect of time and initial concentration on the adsorption of copper

Figure 1 displays the relationship between time and the amount of copper adsorbed, expressed as a percentage. The x-axis represents time in minutes, ranging from 0 to 45 minutes. The y-axis shows the amount adsorbed as a percentage, spanning from 0% to 60%.

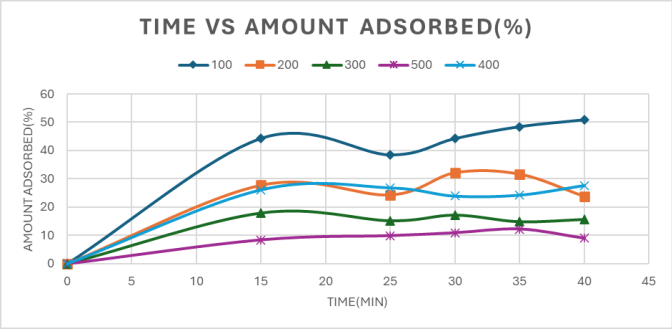

Fig. 1: % Amount of copper adsorbed at time(min)

Figure 2 shows the Freundlich isotherm model for an adsorption process. The Freundlich model is commonly used to describe the adsorption of solutes from a liquid to a solid surface. It is represented as log qe against log Ce.

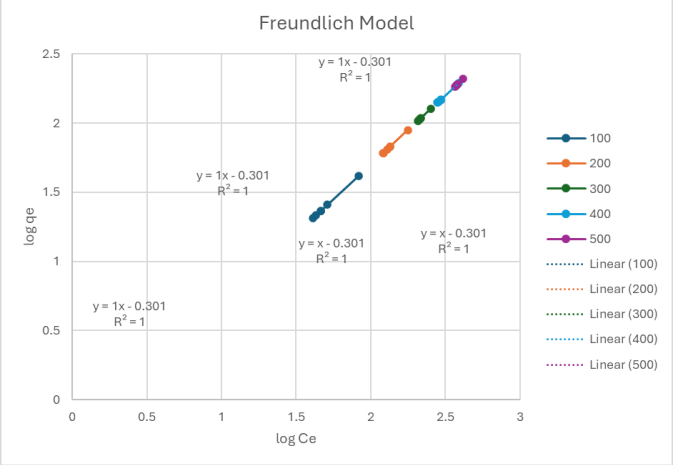

Fig. 2: Freundlich Model log Ce versus log qe

Figure 3 shows the Langmuir isotherm model for an adsorption process. The Langmuir model is widely used to describe adsorption of molecules onto a solid surface at constant temperature. It is represented as 1/qe against 1/Ce.

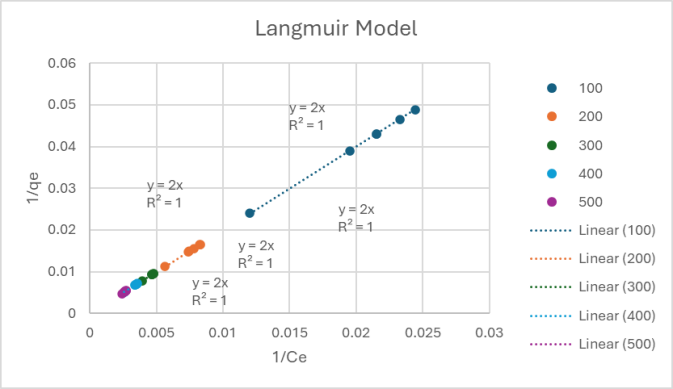

Fig. 2: Langmuir model 1/qe versus 1/Ce

Figure 4 illustrates the Pseudo First Order kinetic model for an adsorption process. The model is used to describe the rate of adsorption based on the adsorption capacity.

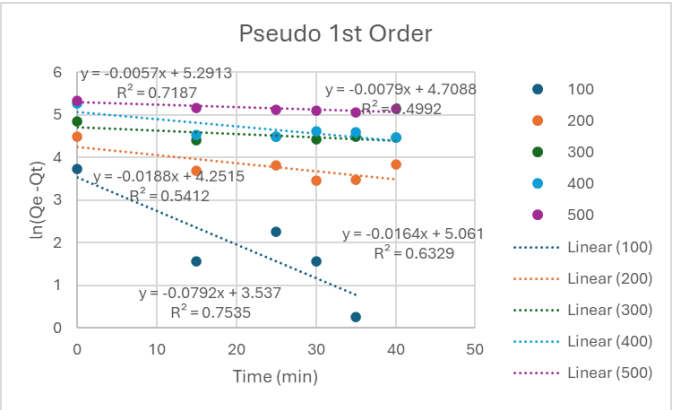

Fig. 3: Pseudo 1st order, ln(Qe - Qt) vs time

Figure 5 shows the Pseudo Second Order kinetic model for an adsorption process. The model is used to describe the rate of adsorption based on the adsorption capacity of the solid phase.

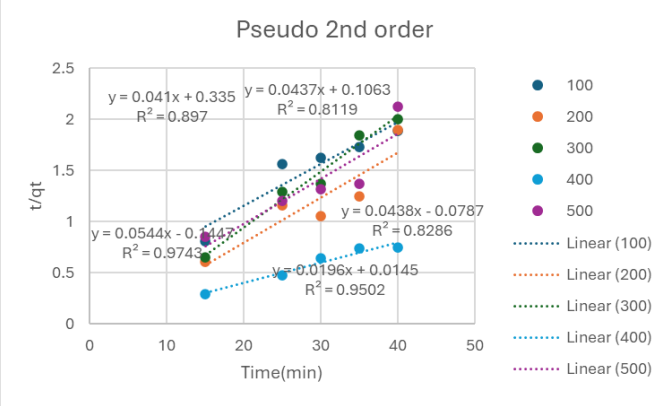

Fig. 4: Pseudo 2nd order, t/qt vs time

Figure 6 below represents the qt at different concentrations and contact time. It is used to find the adsorption capacity.

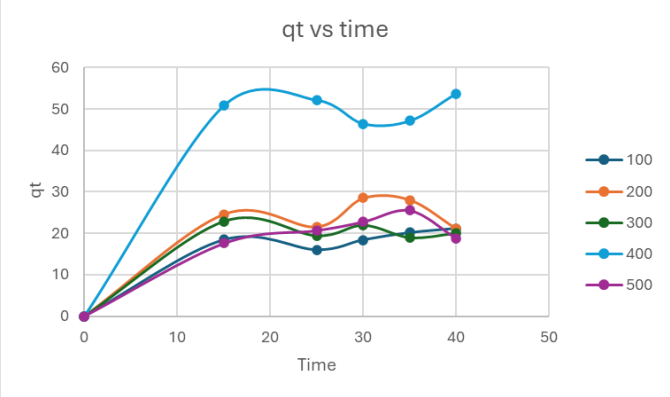

Fig. 5: qt versus time

Table I below shows comparisons between the experimental qe, 1st order qe, and 2nd order qe, to help choose which model is best fit for the obtained results.

TABLE I: COMPARISONS OF QE VALUES

CONC(ppm)	qe	qe	qe
	PFO	PSO	Experimental
100	316.28	24.39	21.03
200	177.79	22.83	21.10
300	513.14	18.38	20.00
400	120.59	51.02	53.74
500	195.46	22.88	18.80

Table II compares of R^2 values between Pseudo first and second order to conclude that this system followed Pseudo second order model.

TABLE II: MODEL SELECTION BASED ON THE COEFFICIENT OF DETERMINATION

Kinetic Model	Correlation coefficient
PFO	R^2
100ppm	0.7535
200ppm	0.5412
300ppm	0.4992
400ppm	0.6329
500ppm	0.7187
AVG value	**0.6291**
PSO	R^2
100ppm	0.897
200ppm	0.8288
300ppm	0.9743
400ppm	0.9502
500ppm	0.8119
AVG value	**0.8924**

B. Morphological properties of adsorbents based on SEM

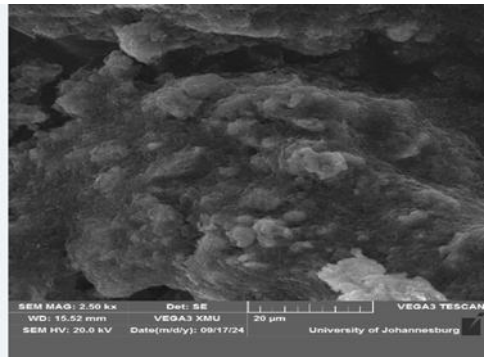

Fig. 7: SEM image of raw bentonite clay

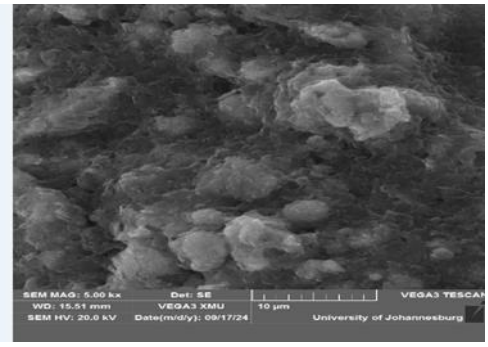

Fig. 8: SEM image of activated bentonite

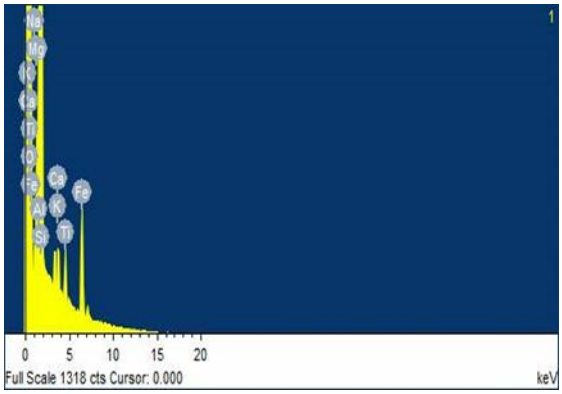

Fig. 9: EDS results of raw bentonite

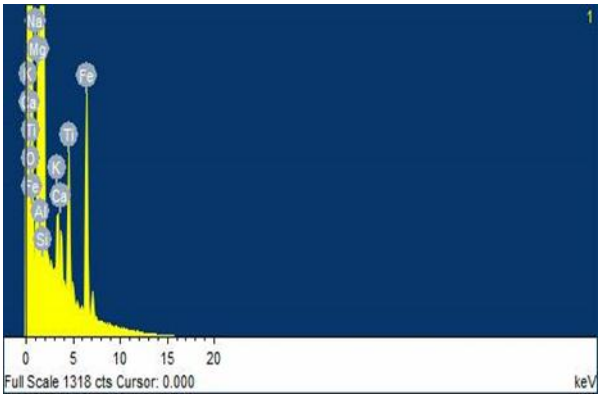

Fig. 10: EDS results of activated bentonite

C. Discussion of results

The highest concentration tested, at 500 ppm, exhibited the lowest percentage of adsorption, reaching a maximum of approximately 12%. This indicates that raising the concentration past a certain level might not increase adsorption rates, likely because the adsorption sites are saturated. All concentrations displayed a quick rise in adsorption during the first 15 minutes, followed by a period where the rates either stabilize or vary a bit. This shows that most adsorption happens early on, with less significant gains over time. The findings imply that adsorption efficiency does not directly relate to concentration, as lower concentrations, especially 100 ppm, achieved a higher percentage of adsorption.

Moving on to the isotherms, figure 2, which is the Freundlich model. The Freundlich isotherm model illustrated in this graph offers strong support for the adsorption characteristics of the investigated system. The relationship between log qe and log Ce reveals a highly consistent linear correlation across all five experimental concentrations (100-500), with each series(conc) aligning perfectly with the model, as evidenced by an R^2 value of 1 for all trendlines. This remarkable linearity indicated that the Freundlich model effectively captures the adsorption dynamics throughout the full spectrum of concentrations analysed. The ideal alignment with the Freundlich model indicated that the adsorption process is advantageous, and that the adsorbent possessed a heterogeneous surface featuring binding sites with differing affinities. This property is advantageous for scenarios that necessitate uniform adsorption performance across a range of concentrations. Additionally, the model's strong predictive capability, demonstrated by the high R^2 values, offered a dependable framework for estimating adsorption capacities at various equilibrium concentrations, which was essential for the design and optimization of processes in practical applications.

Figure 3, which is the Langmuir model. The plot shows 1/qe (inverse of adsorption capacity) versus 1/Ce (inverse of equilibrium concentration). All five concentration (100, 200, 300, 400, and 500 ppm) exhibited linear relationships, with each line having an equation of $y = 2x$ and a perfect coefficient of determination ($R^2 = 1$). The steady slope at all concentrations indicated that the adsorption process closely aligns with the Langmuir isotherm model. This consistent slope across all concentrations suggested that the adsorption process followed the Langmuir isotherm model very closely, indicating a monolayer adsorption on a homogeneous surface with no interaction between adsorbed molecules. The linear relationship and perfect fit to the Langmuir model suggested that this system could be reliably used for predicting adsorption behaviour at various concentrations within the tested range.

Figure 4, Pseudo 1st order model graph. The plot shows ln(Qe-Qt) versus time in minutes. These series of concentrations showed negative slopes, all in agreement with the pseudo-first-order model by presenting decreasing rates of adsorption with time. However, the goodness of fit varied greatly among the concentrations in the range from 0.4992 to 0.7535, hence giving moderate to poor fits to the model. The 100-ppm concentration had the steepest slope at -0.0792 and a better fit with an R^2 of 0.7535 than the other concentrations. This indicated that the adsorption only at 100 ppm aligns more with pseudo-first-order kinetics. On the other hand, the 400-ppm concentration had the shallowest slope at -0.0057 and a lower fit with an R^2 of 0.7187. Different slopes at various concentrations suggested that the rate of adsorption changes. Higher concentrations usually have slower rates, indicated by shallower slopes. This might mean that as concentration goes up, the adsorption process becomes more complicated or faces more resistance. While the pseudo-first-order model provides some insight into the adsorption process, the poor to moderate fits and varying parameters across concentrations indicate that the adsorption kinetics in this system are more complex than what can be fully captured by this simple model.

The Pseudo Second Order kinetic model, Figure 5 showed different adsorption behaviours according to each of the experimental concentrations. Relationship between t/qt vs time for the greatest part of the series usually follows a linear pattern. The 400-ppm showed the best fit to the model with an R^2 of 0.9743 and the steepest slope (0.0544), suggesting faster adsorption kinetics. In contrast, the 100-ppm concentration has a lower R^2 value of 0.8286 compared to 400ppm. The slopes of the trend lines changed a lot across different concentrations, with values from 0.0196 at 400 ppm to 0.0544 at 200 ppm. This difference indicated that the adsorption rate constant and the maximum adsorption capacity depend on the starting concentration. The differences in slopes and y-intercepts among the series indicated varying adsorption rates and initial adsorption capacities under different experimental conditions. The adsorption capacity is proportional to the number of active sites occupied on the adsorbent.

Figure 6, which illustrates the relationship between (qt) and time for various concentrations from 100 to 500 ppm. The adsorption process showed distinct patterns across different concentrations over a 40-minute period. The 400-ppm concentration exhibits the highest overall adsorption capacity, reaching a peak of about 55mg/g at around 15 minutes. It demonstrated a rapid initial increase followed by fluctuations,

suggesting a dynamic equilibrium. The 100, 200, 300, and 500 ppm concentrations showed similar patterns, with adsorption capacities clustering between 20 and 30mg/g. These concentrations displayed a quick initial uptake within the first 15 minutes, followed by slight variations or plateaus. 500 ppm concentration, despite being the highest, did not result in the greatest adsorption capacity. This could indicate a saturation effect or competition for adsorption sites at higher concentrations. The non-linear relationship between concentration and adsorption capacity, particularly evident with the 400-ppm outlier, suggests complex adsorption mechanisms that may involve multiple layers, varying binding energies, or adsorbent surface heterogeneity.

According to the table 1 shown above , the qe value for pseudo second order model was the one closest to the experimental qe value and that of pseudo first order was further away. The pseudo second being close means that it was a better model fit. Also, it suggested chemisorption, involving valence forces through sharing or exchange of electrons between the adsorbent and adsorbate. It may also indicate that the adsorption process was more complex than simple physical adsorption, possibly involving multiple steps or interactions between the adsorbate and adsorbent. On the other , Table 2 is an indication of the R^2 values for both pseudos' first and second order models and it was another indication that this was governed by chemisorption because the highest value is that of the pseudo second order which was found as average of about 0.89.

For Tables 3 & 4(raw & activated, respectively, the natural bentonite clay sample has a typical clay mineral composition, where SiO_2 is up to 66.60% and Al_2O_3 is present at 16.64%, in the normal tetrahedral-octahedral-tetrahedral structure of the montmorillonite. This base material showed a good balance of exchangeable cations like Na_2O at 1.36%, CaO at 1.88%, and MgO at 3.21%, reflecting strong natural swelling and adsorption capabilities. The value of Fe_2O_3 was 8.04%, within the clay range.

By contrast, the bentonite modified by magnetite showed essential changes in its composition, and the most important among the changes was the increase in the content of Fe_2O_3 to 46.53%. This growth was evidence of the successful inclusion of magnetite into the clay structure. The main clay components decreased proportionally: SiO_2 dropped to 33.19%, while Al_2O_3 dropped to 10.86%. This drop was mostly due to the diluting effect from the added magnetite rather than structural degradation, as the Si:Al ratio remained relatively consistent between both samples. The modification process has notably affected the exchangeable cation composition, with Na_2O decreasing to 0.56% while CaO increased to 3.35%. This shift in cation balance suggested that significant ion exchange occurred during the modification process. The modified sample also showed the appearance of new elements such as Cr_2O_3 (0.15%) and increased TiO_2 (1.03%), which may have been due to introduction of the magnetite source material. The high content of iron oxides in the modified sample suggested superior performance in magnetic separation and recovery, thus a very environmentally applicable method for water treatment and contaminant removal. Despite the significant magnetite loading, the activated sample kept the basic silica-alumina framework, indicating successful alteration without destroying the crucial clay structure. This preservation was important because it showed that the changed material gained new functional capabilities while retaining some of the original bentonite's advantageous qualities.

Figure 7 represents the surface of raw, natural bentonite clay. The morphology was mostly uniform and homogeneous. Essentially, this comes from a flaky-layered structure that characterizes the texture in most clay minerals. Such consistent morphology suggested the predominance of a basic aluminosilicate framework in defining the composition of natural bentonite clay without the addition of any significant external components. Figure 8 shows the magnetite-modified bentonite which displayed a very different surface morphology, with the texture being very complex and heterogeneous. Well-differentiated aggregates, as well as clusters of particles dispersed in the clay matrix were present. The mentioned enlargement in textural complexity and variation in brightness or contrast within the image indicated the successful inclusion of magnetite particles within the structure of bentonite, which modified the superficial characteristics of the clay. Figure 9 gives an even finer-scale view of the microstructure from modified bentonite clay. With the higher magnification, it can be observed that the surface exhibited a greater degree of particle agglomeration with a more heterogeneous distribution than what has been provided by the previous images. Such complexity on the smaller scale could suggest intimate integration of the magnetite component into the supporting clay framework to realize hybrid material properties from both the clay and magnetic properties. Figures 10 and 11 represent the EDS spectra of raw and activated bentonite clay respectively. From figure 10 to 11, it is seen that the peak of Fe has dramatically changed overtime, there occurred a sharp increase which indicated that the clay from figure 10 has been magnetised to figure 11. This complemented the XRF analysis as well which henceforth proved and showed that the clay has been magnetised

IV. Conclusion

The investigation confirmed that magnetized bentonite clay particles are highly effective in removing copper ions from wastewater, achieving an impressive 60% removal efficiency under optimal conditions. The study identified that adsorption is significantly influenced by contact time and initial copper concentration, with the most effective adsorption occurring within 45 minutes. Kinetic analysis revealed that the adsorption process was best described by the pseudo-second-order model, indicating a strong interaction between the copper ions and the MBCP, concluding chemisorption adsorption. Additionally, the magnetic properties of MBCP facilitated easy separation from treated water, enhancing

operational efficiency. Furthermore, the use of Freundlich and Langmuir isotherm models demonstrated that the adsorption behaviour was consistent with these theoretical frameworks, indicating a heterogeneous surface with varied affinities for copper ions. This research not only demonstrated the feasibility of using MBCP for copper recovery but also contributed to sustainable practices in wastewater management. Future studies should focus on scaling this method for broader industrial applications and exploring its effectiveness against other heavy metals.

ACKNOWLEDGMENT

The authors are grateful for the financial support received from the Faculty of Engineering and the Built Environment at the University of Johannesburg.

REFERENCES

[1] Afrodita Zendelska, Mirjana Golomeova, Krsto Blazev, Krstev, B., Blagoj Golomeov and Aleksandar Krstev (2015). Adsorption of copper ions from aqueous solutions on natural zeolite. Environment Protection Engineering, [online] 41(4). doi:https://doi.org/10.37190/epe150402. https://doi.org/10.37190/epe150402

[2] Nthambeleni Mukwevho, Elvis Fosso-Kankeu, Frans Waanders, Neeraj Kumar, Suprakas Sinha Ray, Xavier Yangkou Mbianda. 2019. Evaluation of the photocatalytic activity of Gd2O2CO3.ZnO.CuO nanocomposite used for the degradation of phenanthrene. Springer Nature Applied Sciences. https://doi.org/10.1007/s42452-018-0012-0. 1-10.

[3] Elvis Fosso-Kankeu, Frans B. Waanders, Frederik W. Steyn. 2017. Removal of Cr(VI) and Zn(II) from an aqueous solution using an organic-inorganic composite of bentonite-biochar-hematite. Desalination and Water Treatment. 59: 144-153. https://doi.org/10.5004/dwt.2016.0059

[4] E. Fosso-Kankeu, F. Waanders, E. Maloy. 2016. Copolymerization of ethyl acrylate onto guar gum for the adsorption of Mg (II) and Ca (II) ions. Desalination and Water Treatment. doi: 10.1080/19443994.2016.1165147: 1-10. https://doi.org/10.1080/19443994.2016.1165147

[5] Elvis Fosso-Kankeu, Frans. B. Waanders, Frederik W. Steyn. 2015. The Preparation and Characterization of Clay-Biochar Composites for the Removal of Metal Pollutants. 7thInternational Conference on Latest Trends in Engineering and Technology (ICLTET' 2015), November 26-27, 2015 Irene, Pretoria (South Africa). Editors: E. Muzenda and T Yingthawornsuk. ISBN: 978-93-84422-58-5.

[6] A. Manyatshe, E. Fosso-Kankeu, D. van der Berg, N. Lemmer, F. Waanders, H. Tutu. 2017. Dispersion of inorganic contaminants in surface water in the vicinity of Potchefstroom. Physics and Chemistry of the Earth. 100: 86-93. https://doi.org/10.1016/j.pce.2017.04.008

[7] E Fosso-Kankeu. 2018. Synthesized af-PFCl and GG-g-P(AN)/TEOS hydrogel composite used in hybridized technique applied for AMD treatment. Journal of Physics and Chemistry of the Earth. 105: 170-176. https://doi.org/10.1016/j.pce.2018.02.015

[8] E. Fosso-Kankeu, A.F. Mulaba-Bafubiandi, L.A. Piater, M.G. Tlou. 2016. Cloning of the cnr operon into a strain of Bacillaceae bacterium for the development of a suitable biosorbent. World Journal of Microbiology and Biotechnology. DOI 10.1007/s11274-016-2069-5. https://doi.org/10.1007/s11274-016-2069-5

[9] E. Fosso-Kankeu, A.F. Mulaba-Bafubiandi, T.G. Barnard. 2014. Establishing suitable conditions for metals recovery from metal saturated Bacillaceae bacterium using experimental design. International Biodeterioration and Biodegradation. 86: 218-224. https://doi.org/10.1016/j.ibiod.2013.09.022

[10] Shah, K.H., Ali, S., Waseem, M., & Naz, S. (2019). Native and Magnetic Oxide Nanoparticles (Fe3O4) Impregnated Bentonite Clays as Economic Adsorbents for Cr (III) Removal. Journal of Solution Chemistry, 48(10), pp. 1640-1656. https://doi.org/10.1007/s10953-019-00912-z